Journal of Manufacturing Engineering, March 2015, Vol. 10, Issue. 1, pp 17-26

MICRO STRUCTURAL ANALYSIS OF MOLYBDENUM BASED CERAMIC NANO COATINGS FABRICATED BY PLASMA VAPOUR DEPOSITION

[*]Jinnah Sheik Mohamed[1] and Selvakumar N[2]

[1] Asst.Professor in Mechanical Engineering, National College of Engineering, Maruthakulam, Tirunelveli
[2] Professor in Mechanical Engineering, Mepco Schlenk Engineering College, Sivakasi.

ABSTRACT

Coatings and surface engineering are used to protect manufactured components from thermal or corrosive degradation, impart wear resistance and hardness to the surface while retaining the toughness and ductility of the bulk component, also enhance the aesthetic and decorative appeal. In this work Molybdenum based ceramic Nanocomposite (MoSi2-SiC) coating was deposited on the surface of Mild steel substrate by Plasma Vapour deposition (PVD) Method in RF Magnetron Sputtering process. The thickness of the nanocoatings was varied as 50nm, 75 nm and 100 nm. X- ray diffraction (XRD) and Scanning electron microscopy (SEM) were used to characterize the microstructures of Mo based ceramic coating. The surface hardness of substrate and coating were determined using a Vickers microhardness tester. Corrosion resistance analysis was also carried out using acidic bath environment by weight loss method. The results indicated that as prepared Mo based coating was mainly composed of Mo, Si and C phases. The coating presented a dense layered structure and thereby surface hardness of coated substrates was as high as the uncoated substrates. The microhardness along the cross-section gradually increased from substrate to coating. The corrosion resistance of MoSi2-SiC coating was far better than that of substrate.

Keywords: *Nanocoating, Sputtering, Corrosion Resistance, SEM, $MoSi_2$-SiC*

1. Introduction

Physically vapor deposited (PVD) thin films are an industrially important class of materials which find use in a wide field of applications, from protective coatings in mechanical engineering for tooling and cutting operations [1], heaters [2] in electronic components, diffusion barrier coatings in energy devices [3–5], and optical applications in solar selective absorbers. Due to its superior physical and mechanical properties, Molybdenum based ceramic coating has found a wide range of applications, such as plasma faced components in fusion reactors, $MoSi_2$-SiC coatings on semiconductor substrates in microelectronic systems, coatings on heat pipes, cladding of nuclear fuel, radiation shields for propulsion and space nuclear power systems, corrosion-resistant coatings. The objective of this work is to investigate the microstructural and corrosion behavioral properties of $MoSi_2$-SiC coatings formed at different combinations such as 5%, 10%, 15% and 20% SiC with $MoSi_2$ in reactive RF Magnetron sputtering process. The structural morphology of the coatings was explored by XRD, scanning electron microscopy (SEM), FT-IR, Atomic force microscopy (AFM) and the composition of the deposits was analyzed by energy dispersive X-ray analysis (EDX). The corrosion resistance of $MoSi_2$-SiC coatings was evaluated by acidic bath method by dipping the mild steel substrate in different acid environment (H_2SO_4, HCL, and HNO_3) with various concentrations such as 0.01N, 0.1N and 0.2N for 86.4ks in room temperature. The results reveal that the prepared ceramic Nanocomposites are very good inhibitors with little concentration. However, the value of percentage inhibition efficiency (IE) was dependent on the concentration of inhibitors in 0.05–0.2 N.The micro hardness of the coatings was determined by Vickers hardness apparatus with 0.1 kg load. Micro hardness values increased with CMC addition in the Mild steel. Response Surface methodology (RSM) was applied to optimise the corrosion parameters to attain maximum inhibition efficiency.

2. Experiment

Materials

The metal powders Molybdenum, Silicon, Carbon and chemicals sulphuric acid, hydrochloric acid and nitric acid were purchased from E-Merck and used as such. MoS_2 was used as lubricant for preparing NC

*Correspondina Author - E- mail: driinnah@nce.ac.in

pellets in Die set assembly. Double deionised water was used for all processes in corrosion studies.

2.2 Synthesis of Nanocomposites

The composite is prepared in three different elements with Molybdenum, Silicon and Carbon which forms MoSi2 as primary matrix and SiC as secondary matrix. In this present study, elemental powders of Mo (99.9%, 1-2µm), Si about 20µm and fine Carbon black (99.9%, 45 µm) are mixed in the desired proportions in a Glove box (Model: M Braun, AB Star-Germany) under argon gas atmosphere and sealed in a cylindrical WC vial together with 50 WC balls of 10 mm in diameter so as to obtain SiC of 5%, 10 %, 15% and 20 % by weight with MoSi2 powder composite. The ball milling experiments are carried out using high-energy ball mill (Model: Pulversitte 6, Germany) at a rotation speed of 300 rpm for 60 hrs of high temperature milling to attain the final by-product. [6]

3. Microstructural Analysis of Nanocomposite

3.1 FT-IR studies

Infrared Spectroscopy is a versatile and common method for characterization of chemical bonds. This technique is based upon the simple fact that a chemical substance shows marked selective absorption in the infrared region. Figure 1(a) shows the details about the vibrational frequencies of $MoSi_2$-10%SiC composite recorded in solid mode of FT-IR spectrometer. This predicts that characteristic peaks are obtained in the region of 1030 cm^{-1} , 853 cm^{-1} and 864 cm^{-1}.

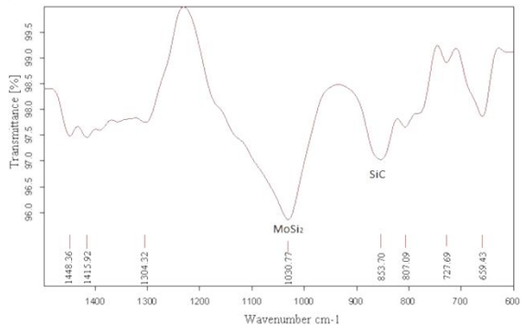

(a) $MoSi_2$ -10 SiC

The peak at 1030 cm^{-1} is attributable to the $MoSi_2$ and the peak at 853 cm^{-1} is assigned to SiC for 10%SiC composite and peak at 864 cm^{-1} for 15% SiC composite. The increase in % of SiC influences the absorption peaks of $MoSi_2$ and SiC (1030 $cm^{-1}$and 864 cm^{-1}) which are slightly shifted because of hard nature of secondary particle (SiC) than primary matrix ($MoSi_2$). (Wei et al., 2009 and Selvakumar, et.al. 2011)[7]

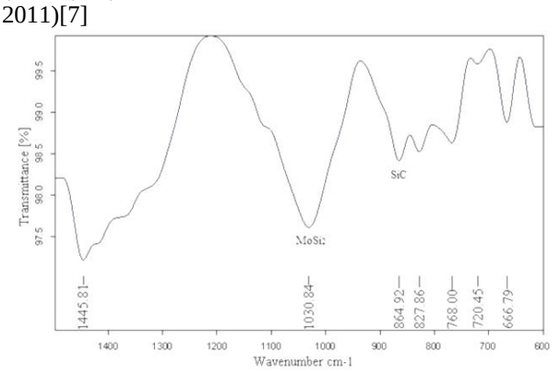

(b) $MoSi_2$ -15 SiC

Figure 1(a-b): FTIR image of $MoSi_2$-SiC composites

Figure 1(b) predicts that vibrational frequency of MoSi2 is obtained in the peaks of 1030 cm-1 and for SiC peak is 864 cm-1 for MoSi2-15%SiC. Because of hard nature of SiC, FT-IR peaks shifted while increasing the content of SiC from 10% to 15%.Thus FT-IR images confirmed the formation MoSi2 and SiC when individual elemental powders are milled in desired proportions as per the procedure described in Materials and Manufacturing methods section.

3.2 Raman spectroscopic analysis

Raman Spectroscopy predicts molecular vibrational information that is inactive in the infrared region because of molecular symmetry. It uses visible or UV radiation rather than IR radiation. It was carried out to find the vibrational, rotational and other low frequency modes in a system (Model: Nexus 670, TEC,USA). Figure 2 predicts that Raman shift for $MoSi_2$ is obtained in 502 cm^{-1}. But while increasing the weight percentage of SiC, intensity of Raman shift increases as shown in the figure[8]

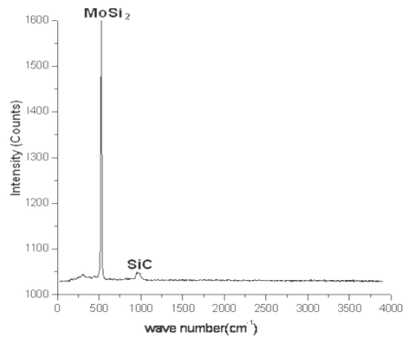

(a) MoSi2 -10 SiC

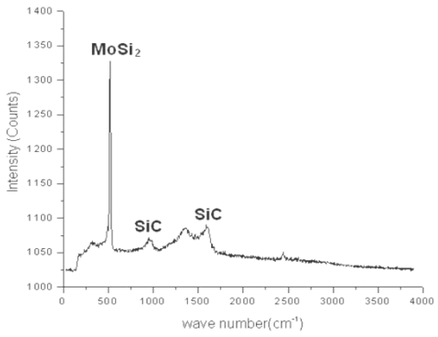

(b) $MoSi_2$ -15 SiC

Figure 2(a-b): RAMAN image of $MoSi_2$-SiC composites

Figure 2(a-b) shows the intensity of SiC in ordinate axis for MoSi2 -10%SiC is 1045 counts and increases gradually up to 1084 counts for MoSi2 -15%SiC.The scattered intensities of peak height on the spectrum are then converted into scattering co efficient by dividing the recorded height of the sample peak by average height of the dual traces of MoSi2 peak. By standard reference, peaks are obtained in cells of the same value (502 cm-1).This study is used to analyse the composition (Mo, Si, C) of samples after every processing step.(Kin-Tak et al.,2010).

3.3. XRD analysis

The XRD patterns of $MoSi_2$ & SiC NC are represented in Figure3 (a-b) for two different combination of Nanocomposite such as 10% and 15% SiC with $MoSi_2$. A single distinct peak appears at 2θ = 41.4° which indicates the crystallinity of SiC that is resembled with JCPDS file No. 29-1129 (Naveen et al.,2010) and no other peaks appearing over the scan range from 30° and 45°. According to XRD pattern, the peaks corresponding to SiC are appeared additionally at 2θ = 59.1° and 74.5° (Figure3).It is observed that peak appears at 2θ = 29.8° and 49° which is identified as the $MoSi_2$ reflection and clear that the 2θ peak characteristics for $MoSi_2$ and SiC are obtained in the same position for 10% and 15% SiC combinations.[9] Also, from XRD pattern of the composites, the crystalline size of the samples is calculated using Debye Scherer equation (1).

3.4 SEM/EDAX results

Scanning Electron Microscopy equipped with energy dispersive X ray spectroscopy analysis (SEM-EDX PHILIPS XL 30) was used for investigation of microstructure and elemental analysis of the sample obtained at different conditions.

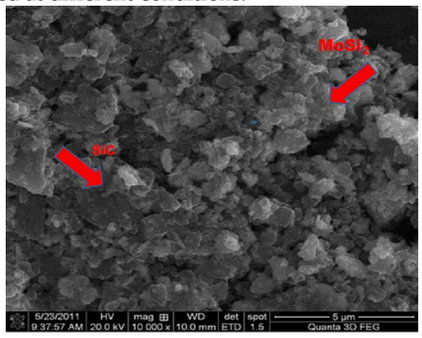

Before coating

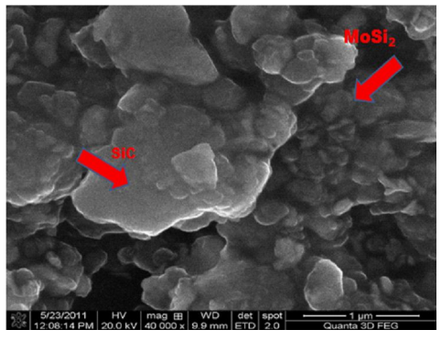

(b) After Coating

Figure 4 (a-b): SEM image of $MoSi_2$-SiC composites

The morphology of the synthesized MoSi2-SiC composite and different phases were observed by scanning electron microscopy. Prior to examination all samples are ion sputtered with gold to enhance the charging of particles. Figure 4(a-b) shows the SEM images of Nanocomposites in which MoSi2-SiC are identified as two flattened different phases. This is because of crushing the base powder along with secondary particles for prolonged time. Figure 4(a)

provides the image of $MoSi_2$-10%SiC Nanocomposite and represents clear visibility of individual powder particles. Figure 4(b) shows the SEM image of $MoSi_2$-15%SiC composite powder which is milled in high energy ball mill for about 60 *hrs*. The grey spots on the $MoSi_2$ granule show the deposition of SiC on the $MoSi_2$ matrix. The shape of the $MoSi_2$ particle is appearing like amorphous rock and flaky shape (yuriy et al., 2011). The increase in % of SiC by weight increases the particle sizes of composites because of constant milling time and hard nature of SiC.[10] Energy Dispersive X ray spectroscopic analysis (EDAX) is used for investigation of microstructure and elemental analysis of samples obtained at different conditions.

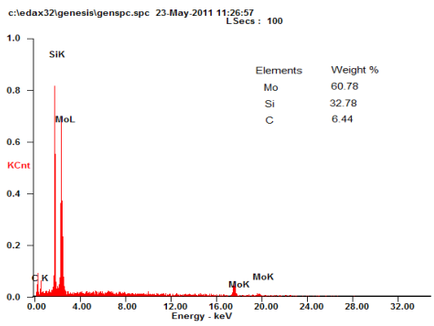

(a) $MoSi_2$ -10 SiC

3.5 Topography of Nanocomposite using AFM

AFM is very important characterization technique to observe the morphological configuration and also the structural analysis in the order of nano range.

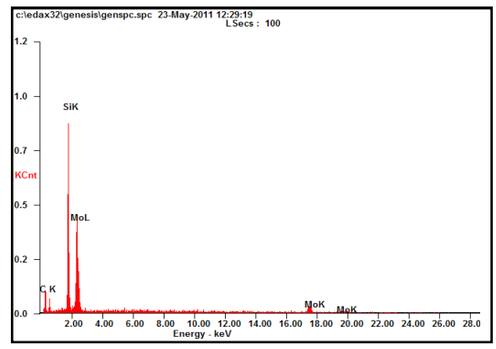

(b) $MoSi_2$ -15 SiC

Figure 5 (a-b): EDAX image of $MoSi_2$-SiC composites

Figure 5(a) gives the elemental information of MoSi2-10SiC in which 60.78% Molybdenum,32.78% Silicon and 6.44% carbon by weight are obtained.

Figure 6(a) exhibits the AFM image of $MoSi_2$-10%SiC composite in two dimensional formats. Particle distribution found in 10 X 10 μm area is explored by drawing a line profile across the 2D image which is represented as red line.[11] Vertical line drawn is indicated by the green line. The surface roughness (R_a) found on red and green line is 11.675 *nm* & 9.600 *nm* respectively (Pavel et al., 2010).

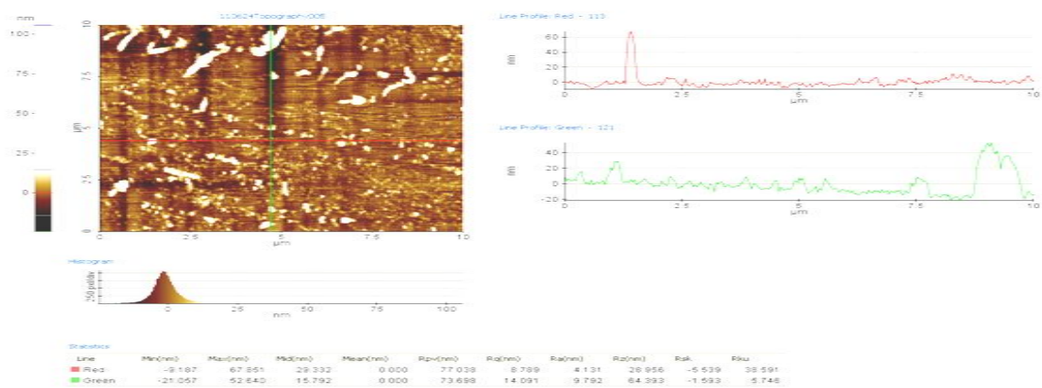

FIGURE 6(b): AFM Topography of the $MoSi_2$ -15 % SiC composite

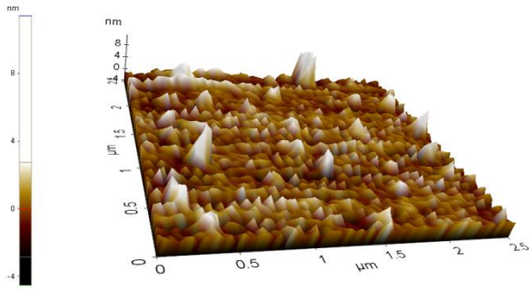

Fig. 6(a): 3D image of AFM Topography

Figure6 (b) exhibits the three dimensional image of AFM topography of 10% SiC Nanocomposite and predicts that the size of the particle is around 8 nm. Figure 6(c) shows the AFM image of CMC containing $MoSi_2$-15%SiC composite of scan size of 10x10 µm observed that the surface roughness and particle size are attained to the maximum of 14.091 *nm* and 12 *nm* respectively.

4. CORROSION BEHAVIOURAL ANALYSIS

4.1 Preparation of coated specimen by sputter deposition

Sputter deposition is a physical vapor deposition (PVD) method of depositing thin films by sputtering process. This involves ejecting material from a target that is a source (MoSi2-SiC) onto a substrate (Mild steel). The mild steel plates of dimensions 75 mm x 25 mm with thickness 2mm were polished with various grades of emery sheets and degreased using acetone solution. The target and substrate are loaded in RF Magnetron sputtering machine. The ceramic coating was deposited on mild steel substrates with $MoSi_2$-5SiC target by adjusting argon gas inlet in RF Magnetron sputtering process. The thickness of the coatings are controlled and varied as 50, 75 and 100 nm**.**

4.2 Preparation of acidic medium

The mild steel plates are cut into small pieces of dimension 25mm x 25mm x 2mm and are dipped in pickling solution (5% H_2SO_4) for 5 minutes and washed with distilled water. After drying, the steel plates are cleaned, polished with various grades of emery sheets and degreased using acetone. The weight of the specimens with absence of ceramic coating were noted and then immersed in glass beaker containing test solution of various concentrations of sulphuric acid (such as 0.05N H_2SO_4, 0.1N H_2SO_4 and 0.2N H_2SO_4), hydrochloric acid (such as 0.5N HCL, 0.1N HCL and 0.2 N HCL) and nitric acid (such as 0.5N HNO_3, 0.1N HNO_3 and 0.2 N HNO_3) separately for 24 hrs. After the time duration, the specimens were removed from the solution and washed thoroughly with distilled water and placed in hot oven for few minutes for drying. Finally the weight was measured. The differences in weight were noted and the percentages in weight loss (WL), corrosion rate (CR) and inhibition efficiency (IE) were calculated using eqs.

$$\%\text{Weight Loss} = \frac{w_i - w_f}{w_i} \times 100 \quad (2.1)$$

Where w_i *and* w_f are initial and final weights of mild steel specimen before and after immersed in acid solution respectively.

$$CR = \frac{87.6W}{DAT} \quad (2.2)$$

Where W, D, A and T are weight loss in mg, metal density in g/cm3, area of steel specimen in cm2, time of exposure of metal specimen in hrs respectively.

$$\%IE = \frac{W_a - W_p}{W_a} \times 100 \quad (2.3)$$

Where W_a and W_p are weight loss in g of mild steel in absence and presence of corrosion inhibitor respectively.

Table-1 Corrosion rate and Inhibition efficiency of Mild steel in *0.05N acid solution of 5% SiC-$MoSi_2$*

Coating Thickness (nm)	Weight Loss (%)			Corrosion Rate (CR)			Inhibition Efficiency (IE) %		
	H_2SO_4	HCL	HNo_3	H_2SO_4	HCL	HNo_3	H_2SO_4	HCL	HNo_3
0	0.480	0.050	0.060	1.736	1.240	1.480	-	-	-
50	0.180	0.020	0.040	0.794	0.490	0.992	54.280	80.000	95.250
75	0.160	0.017	0.032	0.744	0.420	0.793	57.140	99.650	98.640
100	0.05	0.005	0.009	0.248	0.130	0.223	85.710	99.870	99.880

Table-2 Corrosion rate and Inhibition efficiency of Mild steel in *0.1N acid solution of 5% SiC-$MoSi_2$*

Coating Thickness (nm)	Weight Loss (%)			Corrosion Rate (CR)			Inhibition Efficiency (IE)		
	H_2SO_4	HCL	HNo_3	H_2SO_4	HCL	HNo_3	H_2SO_4	HCL	HNo_3
0	6.880	0.370	0.480	30.000	1.736	1.190	-	-	-
50	2.820	0.340	0.390	12.400	1.488	0.960	58.670	14.280	78.250
75	2.270	0.220	0.210	9.920	0.992	0.520	66.940	42.850	82.140
100	1.700	0.188	0.140	7.680	0.843	0.340	74.380	51.420	88.140

Table-3 Corrosion rate and Inhibition efficiency of Mild steel in *0.2N acid solution of 5% SiC-$MoSi_2$*

Coating Thickness (nm)	Weight Loss (%)			Corrosion Rate (CR)			Inhibition Efficiency (IE)		
	H_2SO_4	HCL	HNo_3	H_2SO_4	HCL	HNo_3	H_2SO_4	HCL	HNo_3
0	5.050	4.920	1.230	6.944	5.770	3.050	-	-	-
50	3.320	2.220	1.060	4.488	3.270	2.620	35.360	43.340	68.240
75	2.010	1.730	0.860	3.124	3.120	2.130	55.000	45.920	72.650
100	1.950	1.670	0.590	2.850	2.550	1.460	58.920	55.790	79.890

Table-4 Corrosion rate and Inhibition efficiency of Mild steel in *0.05N acid solution of 10% SiC-$MoSi_2$*

Coating Thickness (mm)	Weight Loss (%)			Corrosion Rate (CR)			Inhibition Efficiency (IE)		
	H_2SO_4	HCL	HNo_3	H_2SO_4	HCL	HNo_3	H_2SO_4	HCL	HNo_3
0	5.77	0.00248	0.138	7.78	0.396	0.263	-	-	-
50	3.60	0.00174	0.113	5.20	0.272	0.056	33.12	31.25	96.56
75	1.62	0.00729	0.966	2.62	0.099	0.043	66.24	75.00	97.81
100	1.03	0.00140	0.854	1.95	0.024	0.017	74.84	93.75	99.79

Table-5 Corrosion rate and Inhibition efficiency of Mild steel in *0.05N acid solution of 15% SiC-$MoSi_2$*

Coating Thickness (mm)	Weight Loss (%)			Corrosion Rate (CR)			Inhibition Efficiency (IE)		
	H_2SO_4	HCL	HNo_3	H_2SO_4	HCL	HNo_3	H_2SO_4	HCL	HNo_3
0	2.538	1.74	4.34	4.44	5.250	0.471	-	-	-
50	1.504	0.322	1.43	2.57	0.322	0.099	41.57	89.62	84.31
75	1.453	0.150	0.19	2.20	0.150	0.740	50.00	94.81	87.91
100	0.343	0.042	0.04	0.49	0.042	0.024	88.76	98.58	91.54

5. Results and Discussion

5.1 Hardness Measurement

The Hardness value for uncoated mild steel is 122VHN and hardness value is increased from 142 to 168 VHN while increasing the coating thickness from 25 to 100 nm when coated with $MoSi_2$-5SiC. Similarly hardness value gradually increases for all the different combinations of ceramic nanocomposite coatings. Figure 7 shows the hardness value of Mild steel coated with different ceramic nanocomposite for varying coating thickness. It predicts that hardness value is maximum for $MoSi_2$-5SiC with 100 nm coating thickness. Also it gradually increases for all the combinations.[12]

Figure 8 shows the corrosion inhibition efficiency of mild steel with respect to coating thickness for three different acid environments such as Sulphuric acid, Hydrochloric acid and Nitric acid for $MoSi_2$-5SiC and $MoSi_2$-10SiC combinations. It predicts that while increasing the coating thickness from 50 nm to 100 nm the corrosion inhibition efficiency of mild steel plate in sulphuric acid solution at 0.1 N concentration is higher than 0.05N and 0.2N concentrations. But from the figure 8(b) and 8(c), inhibition efficiency of mild steel in

hydrochloric and nitric acids at 0.05N is more than other concentrated solutions for $MoSi_2$-5SiC combination. Figure 8(d), 8(e) and 8(f) reveals that irrespective of the acid environment the 0.05N concentration solution provide the best result of corrosion inhibition for $MoSi_2$-10SiC combination. Moreover in nitric acid solution the inhibition efficiency rate is 95.25% for 50 nm coating thickness, 98.64% for 75 nm thickness and 99.88% for 100 nm thickness.

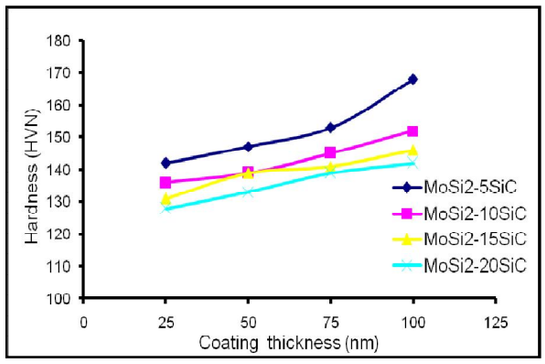

Fig.7 Hardness of Ceramic coated Mild steel

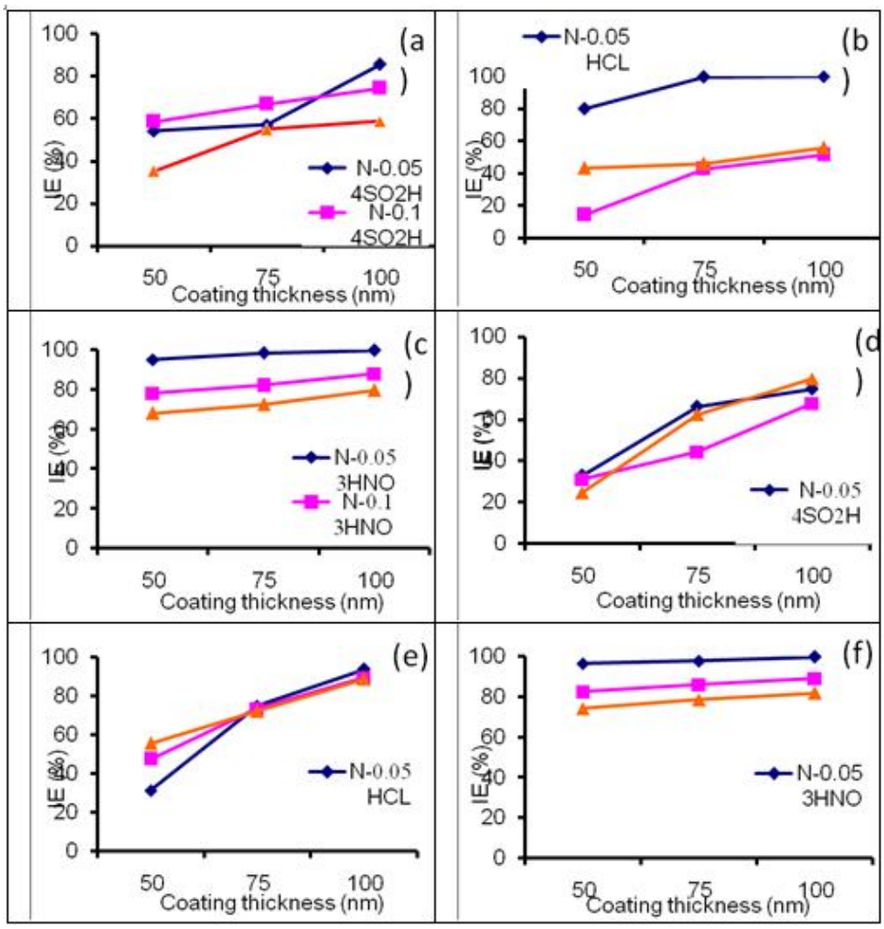

Figure 8: Corrosion inhibition efficiency of mild steel (a) $MoSi_2$-5SiC in H_2SO_4 (b) $MoSi_2$-5SiC in HCL (c) $MoSi_2$-5SiC in HNo_3 (d) $MoSi_2$-10SiC in H_2SO_4 (e) $MoSi_2$-10SiC in HCL (f) $MoSi_2$-10SiC in HNo_3.

5.2 Corrosion of steel in acid medium by weight loss method

The corrosion behaviour of mild steel in various concentrations of acids *H_2SO_4, HCL and HNo_3* is tested by immersing at room temperature for about 24 hrs for different combinations of ceramic Nanocomposite targets. In the presence of *$MoSi_2$*-SiC coating, the ceramic coating is act as corrosion inhibitors. The weight loss in %, corrosion rate and inhibition efficiency are determined for various coating thickness using Eqs. (2.1), (2.2) and (2.3) and given in table 3, 4 & 5. From the table it is clear that the inhibition efficiency is directly proportional to the coating thickness of the ceramic composites.[13] Also weight loss is decreased while increasing the thickness of coating. Corrosion rate is indirectly proportional to coating material thickness. The maximum corrosion inhibition efficiency is 85.71% for *H_2SO_4*, 99.87% for HCL and 99.88% for *HNo_3* for 0.05N concentration in *5% SiC-$MoSi_2$* target.

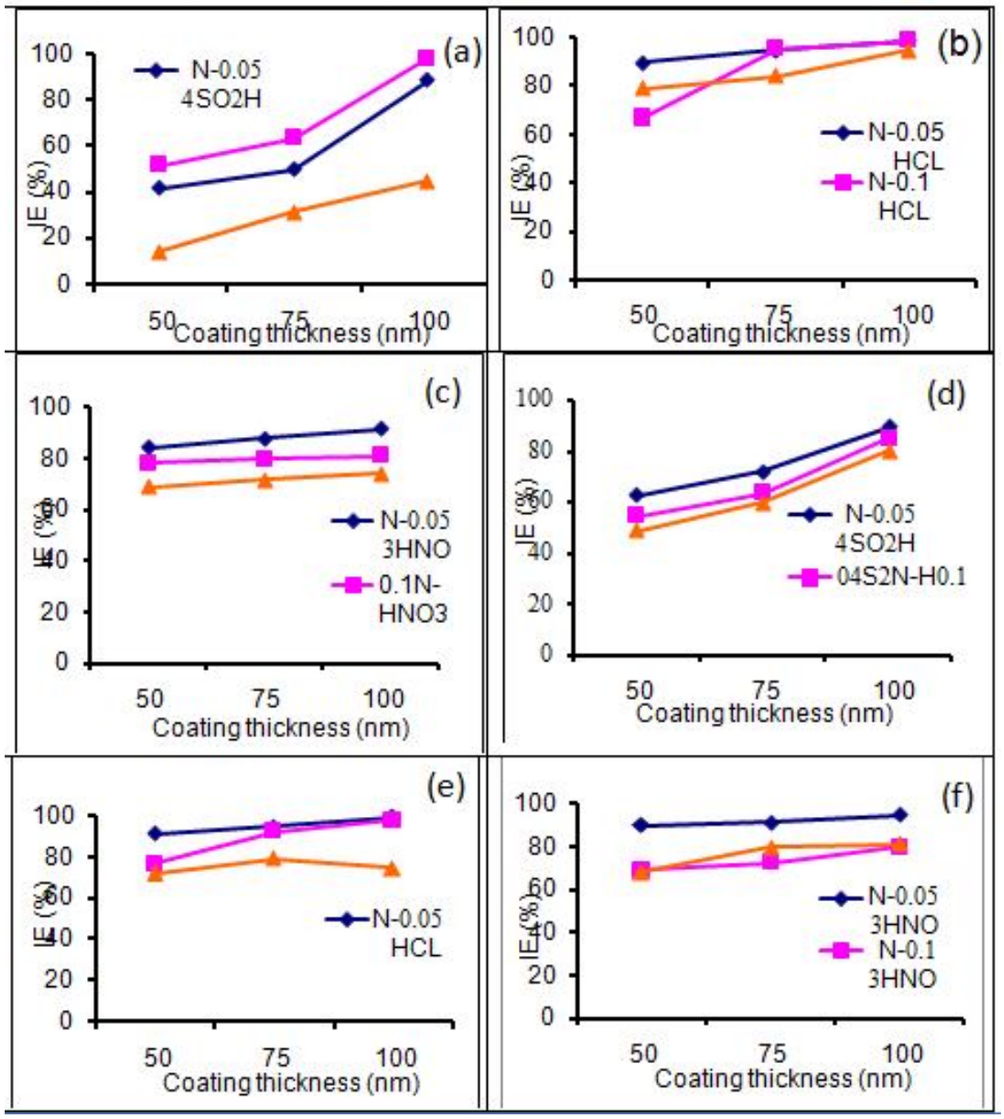

Fig. 9 Corrosion inhibition efficiency of mild steel (a) $MoSi_2$-15SiC in H_2SO_4 (b) $MoSi_2$-15SiC in HCL (c) $MoSi_2$-15SiC in HNo_3 (d) $MoSi_2$-20SiC in H_2SO_4 (e) $MoSi_2$-20SiC in HCL (f) $MoSi_2$-20SiC in HNo_3.

Figure 8 shows the corrosion inhibition efficiency of mild steel with respect to coating thickness for three different acid environments such as Sulphuric acid, Hydrochloric acid and Nitric acid for $MoSi_2$-5SiC and $MoSi_2$-10SiC combinations. It predicts that while increasing the coating thickness from 50 nm to 100 nm the corrosion inhibition efficiency of mild steel plate in sulphuric acid solution at 0.1 N concentration is higher than 0.05N and 0.2N concentrations. But from the figure 8(b) and 8(c), inhibition efficiency of mild steel in hydrochloric and nitric acids at 0.05N is more than other concentrated solutions for $MoSi_2$-5SiC combination. Figure 8(d), 8(e) and 8(f) reveals that irrespective of the acid environment the 0.05N concentration solution provide the best result of corrosion inhibition for $MoSi_2$-10SiC combination. Moreover in nitric acid solution the inhibition efficiency rate is 95.25% for 50 nm coating thickness, 98.64% for 75 nm thickness and 99.88% for 100 nm thickness.

Figure 9 clearly indicates the corrosion inhibition efficiency of mild steel in three different concentrations of acids such as 0.05N, 0.1N and 0.2N in H_2SO_4, HCL, HNo_3 acid environments for $MoSi_2$-15SiC and $MoSi_2$-20SiC combinations respectively. Figure 9(a), 9(b) and 9(c) predicts as far as $MoSi_2$-15SiC is concern 0.1 N concentration offers elevated corrosion inhibition efficiency while increasing the coating thickness from 50 nm to 100 nm in sulphuric acid medium, hydrochloric acid medium and nitric acid medium respectively. Similarly, The inhibition efficiency of $MoSi_2$-20SiC ceramic Nanocomposite coated mild steel substrates is gradually increased from lower coating thickness to higher coating thickness and maximum efficiency of 99.59% is attained at 0.05N HCL acid medium. In addition that corrosion inhibition efficiency is obtained as 94.69% and 89.54% for 0.05N HNo_3 and 0.05N H_2SO_4 respectively.[14] From the above figure 8 and 9, in all the combinations the corrosion rate (CR) is gradually decreased from increasing coating thickness because of the influence of predominant nanocoating layer. Also the percentage in weight loss is reduced in decreased manner when the coating layer thickness is raised in all the cases.

6. Conclusion

Tribological behavior of ceramic Nanocomposites coated on mild steel was investigated. The emphasis of the work was put on the processing–microstructure–property relationships, with the aim of obtaining guidelines to optimize the processing condition for the best tribological performance. The following conclusions were drawn from the study:

Microstructural analysis reveal that while increasing the percentage of SiC by weight, the particle size of the nano composite also increases because of constant milling time of composites and hard nature of secondary matrix than primary matrix, when the SiC content increases from 5 to 20%, the particle size reduction takes more time and hence the particle sizes and roughness values are coarser.

Hardness value is maximum for MoSi2-5SiC with 100 nm coating thickness. Increasing the coating thickness from 25 to 100 nm micro hardness value increases, Also it gradually increases for all the combinations.

It predicts that while increasing the coating thickness from 50 nm to 100 nm the corrosion inhibition efficiency of mild steel plate in sulphuric acid solution at 0.1 N concentrations is higher than 0.05N and 0.2N concentrations.

Also reveals that irrespective of the acid environment the 0.05N concentration solution provide the best result of corrosion inhibition for MoSi2-10SiC combination. Moreover in nitric acid solution the inhibition efficiency rate is 95.25% for 50 nm coating thickness, 98.64% for 75 nm thickness and 99.88% for 100 nm thickness.

In all the combinations the corrosion rate (CR) is gradually decreased from increasing coating thickness because of the influence of predominant nanocoating layer. Also the percentage in weight loss is reduced in decreased manner when the coating layer thickness is raised in all the cases.

References

1. *Lavigne S B Moreau C Jacques R G S (1995), "The relationship between the microstructure and thermal diffusivity of plasma sprayed tungsten coatings", J. Therm. Spray Technol.Vol. 4, 261–267.*

2. *Breslin C B Fenelon A M Conroy K G (2005), "Surface engineering: corrosion protection using conducting polymers", Mater Design,Vol. 26,233–7.*

3. *Liu X Johnson C Li C Xu J Cross C (2008) Int J Hydrogen Energy,Vol.33,189–96.*

4. *Kraljic M Mandic Z Duic Lj (2003) "Inhibition of steel corrosion by polyaniline coatings", Corros Sci Vol. 45,181–9.*

5. *Kilmartin P A Trier L Wright G A (2002) "Corrosion inhibition of polyaniline and poly (o-methoxyaniline) on stainless steels", Synth Metals,Vol.131,99–104.*

6. *Garcia R C Deschka S Hohenauer W Duwe R Gauthier E Kinke J Lochter M Mallener W Plochl L Rodhammer P Salito A (1997), "High-heat-flux loading of tungsten coatings on graphite deposited by plasma spray and physical vapor deposition", Fusion Technol.Vol. 32, 263–276.*

7. *Krishnan K H John S Srinivasan K N Praveen J Ganesan M Kavimani P M (2006) "An overall aspect of electroless Ni–P*

depositions – a review article" Metal Mater Trans A Vol.37A,1917–26.

8. *Oraon B Majumdar G Ghosh B (2007) "Parametric optimization and prediction of electroless Ni–B deposition", Mater Design Vol. 28(7),2138–47.*

9. *Sahoo P Das S K (2011), "Tribology of electroless nickel coatings – a review", Mater Design Vol.32(4),1760–75.*

10. *Krishnaveni K Narayanan TSNS Seshadri S K (2005), "Electroless nickel–boron coatings: preparation and evaluation of hardness and wear resistance", Surf Coat Technol,Vol. 190, 115–21.*

11. *Nguyen T L Garcia B Deslouis C Xuan L Q (2002), "Raman spectroscopy analysis of polypyrrole films as protective coatings on iron", Synth Metals Vol. 32:105–8.*

12. *Denise M L Delamar M Carlos A F (2003), "Application of polypyrrole/ TiO2 composite films as corrosion protection of mild steel", J Electroanal Chem Vol. 540, 35–41.*

13. *Tuken T O zyilmaz A T Yazc B Erbil M (2004), "Electrochemical synthesis of polyaniline on mild steel in acetonitrile-LiClO4 solution", Appl Surf Sci Vol. 236, 292–305.*

14. *El-Sharif M R Su Y J Chisholm C U Watson A (1993), "Corrosion resistance of electrodeposited zinc–chromium alloy coatings" Corros Sci Vol. 35, 1259–65.*

15. *Chao D S Lien C Lee C M Chen Y C Yeh J T Chen F (2008), Appl Phys Lett.Vol. 92, 062-108.*